brought to you by CO

provided by Aaltodoc Publication Arc

Sub-grid Scale Modeling in Large Eddy Simulation with Variable Eddy-Viscosity Coefficient

Javad Taghinia

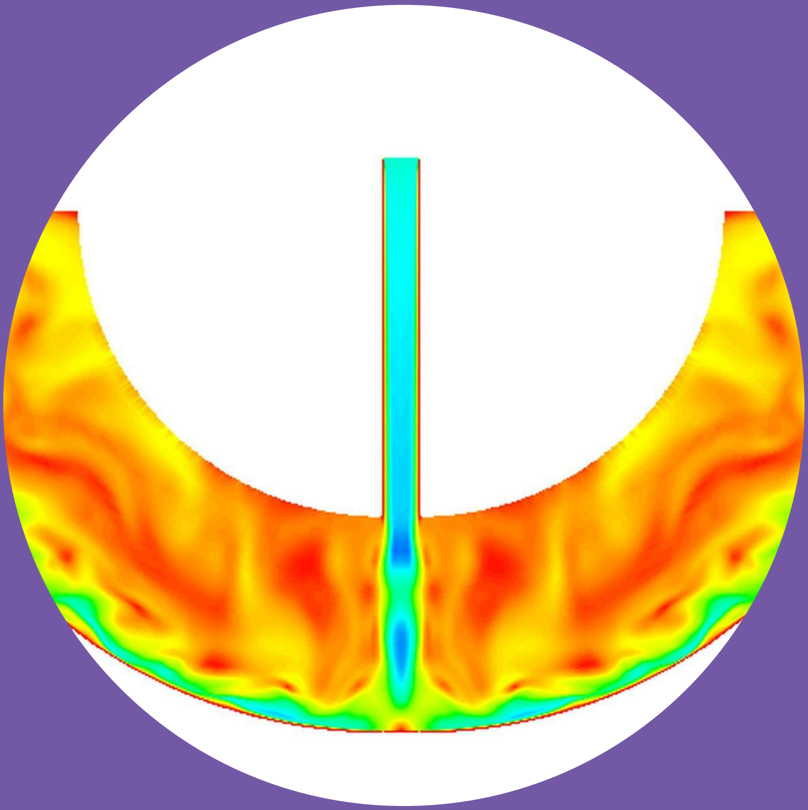

Aalto University

DOCTORAL
DISSERTATIONS

Aalto University publication series
DOCTORAL DISSERTATIONS 195/2015

Sub-grid Scale Modeling in Large Eddy Simulation with Variable Eddy-Viscosity Coefficient

Javad Taghinia

A doctoral dissertation completed for the degree of Doctor of Science (Technology) to be defended, with the permission of the Aalto University School of Engineering, at a public examination held at the lecture hall 172 at Sähkömiehentie 4 (K4 building) on 26th November 2015 at 12.

Aalto University
School of Engineering
Department of Applied Mechanics
Fluid Dynamics Group

Supervising professor
Prof. Timo Siikonen, D.Sc. (Tech.), Aalto University, Finland

Thesis advisor
Dr. Mizanur Rahman, D.Sc. (Tech.), Aalto University, Finland

Preliminary examiners
Prof. Helge I. Andersson, Norwegian University of Science and Technology (NTNU), Norway

Dr. Antti Hellsten, Finnish Meteorological Institute (FMI), Finland

Opponent
Prof. Bernhard Müller, Norwegian University of Science and Technology (NTNU), Norway

Aalto University publication series
DOCTORAL DISSERTATIONS 195/2015

© Javad Taghinia

ISBN 978-952-60-6534-2 (printed)
ISBN 978-952-60-6533-5 (pdf)
ISSN-L 1799-4934
ISSN 1799-4934 (printed)
ISSN 1799-4942 (pdf)
http://urn.fi/URN:ISBN:978-952-60-6533-5

Unigrafia Oy
Helsinki 2015

Finland

NORDIC ECOLABEL
441 697
Printed matter

Aalto University

Aalto University, P.O. Box 11000, FI-00076 Aalto www.aalto.fi

Abstract

Author
Javad Taghinia

Name of the doctoral dissertation
Sub-grid Scale Modeling in Large Eddy Simulation with Variable Eddy Viscosity Coefficient

Publisher School of Engineering

Unit Department of Applied Mechanics

Series Aalto University publication series DOCTORAL DISSERTATIONS 195/2015

Field of research Fluid Dynamics

Manuscript submitted 21 April 2015 **Date of the defence** 26 November 2015

Permission to publish granted (date) 27 October 2015 **Language** English

☐ **Monograph** ☒ **Article dissertation (summary + original articles)**

Abstract

Two new sub-grid scale models for large eddy simulation (LES) are presented; namely zero and one-equation SGS models. These models utilize a novel method for calculating C_u in which the model coefficient is determined from the strain-rate and vorticity parameters. Therefore, it responds to both the shear and vorticity dominated flows that are far from equilibrium. The C_u usually ensures realizability of the resolved normal stresses in question. Unlike the dynamic Smagorinsky model (DSM), both models need only a single filter making them more robust for use in the majority of fluid flow problems. In addition, they require no ad-hoc strategies for achieving the numerical stabilization. Finally, one can save some computational effort in the proposed models, since the test-filtering operation on the SGS stress is not required. In other words, the current models can be considered as a good compromise between accuracy and manageability; particularly, as simple as the original Smagorinsky model and as accurate as the DSM.

The performance of the new models are demonstrated through the comparison with experimental and DNS data of well-documented flows, consisting of fully developed channel flows, indoor airflow, flow over circular cylinder and jet impingement on a concave surface. The predictions are in good agreement with the available data. The test cases are selected such as to justify the ability of the model to replicate the combined effects of low-Reynolds number (LRN), near-wall turbulence and nonequilibrium. Comparisons also indicate that the present model offers competitiveness with the existing SGS models.

Keywords LES, subgrid-scale modeling, variable eddy viscosity, hybrid time–scale, single grid filtering

ISBN (printed) 978-952-60-6534-2 **ISBN (pdf)** 978-952-60-6533-5

ISSN-L 1799-4934 **ISSN (printed)** 1799-4934 **ISSN (pdf)** 1799-4942

Location of publisher Helsinki **Location of printing** Helsinki **Year** 2015

Pages 120 **urn** http://urn.fi/URN:ISBN:978-952-60-6533-5

Preface

The work presented in this thesis was carried out with the Fluid Mechanics group at the Department of Applied Mechanics of Aalto University between 2010 and 2015. I would like to thank my supervising Professor, Timo Siikonen for his support and guidance during the entire process which enabled me to write and finish this work. Secondly, I would like to express my sincere gratitude to my advisor Dr. Mizanur Rahman for his guidance, caring, patience in giving me a new insight into the turbulence phenomenon. I owe a great deal to him in developing my knowledge in fluid dynamics. I also thank Prof. Ramesh Agarwal at Washington University in St. Louis for his valuable comments in preparing manuscripts and publishing papers.

I thank my colleagues, especially Juhaveikko Ala-Juusela in the Fluid Mechanics group for their efforts in creating a positive and supportive working atmosphere. No less important, many thanks to Marisa Lundström for her help in administrative issues.

Finally I would like to express my gratitude to all friends and my family, especially my wife Atefeh, for their love and support during all these years including difficult moments of my life.

Espoo, November 2, 2015,

Javad Taghinia

Contents

Preface **5**

Contents **7**

List of Publications **11**

Author's Contribution **13**

1. Introduction **15**

1.1 Turbulence 15

1.2 Turbulence simulation 17

1.2.1 Direct numerical simulation 17

1.2.2 Reynolds Averaged Navier-Stokes (RANS) 18

1.2.3 Large Eddy Simulation (LES) 19

2. Subgrid-Scale Modeling in LES **21**

2.1 The Smagorinsky Model 21

2.2 The dynamic Smagorinsky model (DSM) 23

2.3 Wall-Adapting Local Eddy-Viscosity (WALE) model 24

2.4 Vreman model 24

2.5 Scale-similarity model 25

3. Mathematical Formulation for the Proposed Models **27**

3.1 Zero–equation Model 27

3.1.1 Eddy–viscosity coefficient C_μ 29

3.1.2 Hybrid time scale T_t 31

3.2 One–equation Model 33

4. Numerical test cases **35**

4.1 Turbulent channel flow 35

4.2 Indoor airflow 39

4.3 Flow past a circular cylinder 43
4.4 Jet impingement on a curved surface 46

5. Conclusions **49**

Publications **51**

Bibliography **115**

List of Abbreviations and Symbols

Symbols

β	thermal expansion coefficient
B	nozzle width
C_μ	eddy–viscosity coefficient
$\bar{C}_s$	Smagorinsky coefficient
D	surface diameter
$\bar{\Delta}$	grid–filter width
$\delta_{i,j}$	Kronecker's delta
Δt	time step
$\tilde{\Delta}$	test–filter width
$\bar{\theta}_i$	grid–filter temperature
$\tilde{\bar{\theta}}_i$	test–filter temperature
G	filter function
g	gravitational acceleration
k	total turbulent kinetic energy
L_{ij}	Leonard stress
ν, ν_T	laminar and turbulent viscosities
Pr	molecular Prandtl number
Pr_{sgs}	sub–grid scale Prandtl number
Re	Reynolds number
ρ	density
$\bar{S}_{ij}$	mean strain–rate tensor
s	radial direction
T	temperature
$\tau_{i,j}$	sub–grid scale stress tensor
U_i	inlet velocity
$\bar{u}_i$	grid–filter velocities
$\tilde{\bar{u}}_i$	test–filter velocities
$\bar{u}_\tau$	friction velocity
$\overline{W}_{ij}$	mean vorticity tensor
y^+	dimensionless wall distance ($\bar{u}_\tau y/\nu$)

Abbreviations

CFD	computational fluid dynamics
DSM	Dynamic Smagorinsky Model
LES	large eddy simulation
$RANS$	Reynolds averaged Navier–Stokes

$RAST$	Rahman–Agarwal–Siikonen–Taghinia
SGS	sub–grid scale

Subscript

i, j	variable numbers
in	inlet condition
out	outlet condition

List of Publications

This thesis consists of an overview with the following publications which are referred to in the text by their Roman numerals.

I Taghinia, J.; Rahman M M.; Siikonen, T.; Agarwal, R. K. A sub–grid scale model with non–traditional eddy–viscosity coefficient. In *7th AIAA theoretical fluid mechanics conference, Atlanta, USA, June 16-20*, 2014, AIAA paper .

II Taghinia, J.; Rahman M M.; Siikonen, T.; Agarwal, R. K. One-equation sub-grid scale model with variable eddy-viscosity coefficient. *Computers & Fluids*, 107, Pages 155–164, 2015 .

III Taghinia, J.; Rahman M M.; Siikonen, T. Heat transfer and flow analysis of jet impingement on concave surfaces. *Applied Thermal Engineering*, 84, 448–459, 2015 .

IV Taghinia, J.; Rahman M M.; Siikonen, T. Simulation of indoor airflow with RAST and SST-SAS models: A comparative study. *Building Simulation*, 8 (3), 297–306, 2015 .

V Taghinia, J.; Rahman M M.; Siikonen, T. Large eddy simulation of flow past a circular cylinder with a novel sub-grid scale model. *European Journal of Mechanics-B/Fluids*, 52, 11–18, 2015 .

Author's Contribution

Publication I: "A sub–grid scale model with non–traditional eddy–viscosity coefficient"

The author carried out the modeling and wrote the manuscript. Dr. Rahman, Prof. Siikonen and Prof. Agarwal made valuable comments on the analyses and manuscript.

Publication II: "One-equation sub-grid scale model with variable eddy-viscosity coefficient"

The author carried out the modeling and wrote the manuscript. Dr. Rahman, Prof. Siikonen and Prof. Agarwal made valuable comments on the analyses and manuscript.

Publication III: "Heat transfer and flow analysis of jet impingement on concave surfaces"

The author carried out the modeling and wrote the manuscript. Dr. Rahman and Prof. Siikonen made valuable comments on the analyses and manuscript.

Publication IV: "Simulation of indoor airflow with RAST and SST-SAS models: A comparative study"

The author carried out the modeling and wrote the manuscript. Dr. Rahman and Prof. Siikonen made valuable comments on the analyses and manuscript.

Publication V: “Large eddy simulation of flow past a circular cylinder with a novel sub-grid scale model”

The author carried out the modeling and wrote the manuscript. Dr. Rahman and Prof. Siikonen made valuable comments on the analyses and manuscript.

1. Introduction

1.1 Turbulence

The vast majority of fluid flows in nature and engineering have turbulent characteristics. Turbulent flows in engineering can be observed in a variety of industrial scales such as chemical and metallurgical processes, ventilation systems and aerodynamics. The analysis of natural phenomena such as sea currents, tornadoes and motion of clouds in the atmosphere deals with an in-depth study of turbulence. There is no clear and exact definition of turbulence to date, although, there is a general definition based on some universal behavior of turbulent flows [1]. Unsteady, irregular and inherently chaotic motions in turbulent flows distinguish such flows from laminar flows. From the mathematical point of view, the appearance of non-linear terms in the Navier-Stokes equations of fluid dynamics produces a level of complexity in the flow field. Highly diffusive and dissipative natures are the two main features of turbulent flows which create a strong mixing, causing transportation of heat and mass in the medium. Turbulent structures can be maintained if there is an energy production mechanism in the system. This energy production process can be injected into the system by an external source or by various mechanisms, working inside the flow domain, such as velocity gradient, rotational motion or density gradient, which leads to the energy cascade through all scales.

An early understanding of turbulence was mostly based on experiments and observations in various common processes found in nature. The mathematical expressions of Reynolds [2] for turbulent motion were among the most influential systematic scientific efforts in this field. After the works of Reynolds, there were a few attempts to describe the mechanism of turbulence. One of the earliest explanations was presented by Richardson [3], who suggested that there is a spectrum of energy ranging from large scales to small scales, and the energy cascade process links all eddies with intermediate sizes. This theory indicated that the kinetic energy of turbulent flows is carried within eddies of various sizes. Based on this idea, Kolmogorov [4] expanded the turbulence theory to the next level by proposing three hypotheses on local isotropy and similarities which explained the underlying mechanism of turbulent structures ranging from the large to the smallest scales. His picture of the turbulence mechanism is the most accurate and universal one to date.

The theory explains that a turbulent flow consists of a wide spectrum of eddy scales and the energy is transferred from larger eddies (structures) to the smaller ones. The similarity hypothesis dictates that the statistics of the small eddies are universal and they are not dependent on properties of the fluid while the large-scale structures are directly affected by the geometry and the boundary conditions. Based on this theory, the size of the smallest scale, the rate of energy transfer between scales, and the rate of dissipation of energy at various scales can be computed.

The Navier-Stokes equations describe the flow field in terms of various physical quantities such as velocity and pressure. All the mechanisms in contributing and creating a turbulent flow are embedded in these equations through various terms. For an incompressible flow with no body forces, the continuity and Navier-Stokes equations read as:

$$\frac{\partial u_i}{\partial x_i} = 0 \tag{1.1}$$

and

$$\frac{\partial u_i}{\partial t} + \frac{\partial u_i u_j}{\partial x_j} = -\frac{1}{\rho}\frac{\partial p}{\partial x_i} + \nu\frac{\partial^2 u_i}{\partial {x^2}_j} \tag{1.2}$$

These equations contain significant variables in determining the flow behavior such as the pressure (p), the velocity vector (u_i), the fluid density (ρ) and the kinematic viscosity (ν). As mentioned earlier, the presence of non–linear terms in the equations makes it a challenging task to provide a general analytical solution (except for some simple flows such as Couette flow). Considering this fact, the numerical procedure should be sought as an alternative in order to find answers for complex flow systems.

1.2 Turbulence simulation

As mentioned in the previous section, analytical approaches are very complicated to employ for complex flow systems or even in a case of a laminar flow. Therefore, with the development in computers and availability of more computational resources, a numerical simulation of fluid flows has proven itself as an alternative and effective approach to tackling the problems in turbulent flows. Over past decades, three main simulation strategies have emerged, namely Direct Numerical Simulation (DNS), Reynolds-Averaged-Navier-Stokes (RANS) and Large eddy simulation (LES). However, there are other methods which are a combination and/or derivative of these three approaches, i.e., Detached Eddy Simulation (DES). These three strategies are briefly discussed in the following sections, however the emphasis is mainly given to an LES which is the targeted topic of this study.

1.2.1 Direct numerical simulation

The most accurate approach in simulating turbulence is the direct numerical simulation (DNS) in which all scales of the flow domain are resolved by solving the Navier–Stokes equations. As the Reynolds number increases, the range of existing eddy scales also gets larger and the need for more grid numbers is inevitable in order to resolve all the scales in the flow field, especially the smallest scales.

In order to get an expression about the size of the smallest scale at which the energy is dissipated, a definition for length scale based on the dissipation rate and viscosity has been devised:

$$\eta = \left(\frac{\nu^3}{\epsilon}\right)^{\frac{1}{4}} \tag{1.3}$$

where ϵ is the dissipation rate and ν is the viscosity. This length scale is *Kolmogorov scale* and is the smallest scale presented in turbulent flows.

The relationship between the required nodes and the Reynolds number is roughly about $Re^{\frac{9}{4}}$. This limitation and the present status of computational resources make DNS impractical for the majority of engineering fluid flow problems which deal with high Reynolds numbers. For example, simulating a car with $Re = 10^6$ with a characteristic velocity of 10 m/s requires about 10^{14} nodes. However, during the last 15 years, there have been some efforts to compute simple cases such as channel flow and backward-facing step flows, which provide valuable information on the nature of turbulent flows.

1.2.2 Reynolds Averaged Navier-Stokes (RANS)

Two of the most important characteristics of turbulent flows are irregularity and chaotic motions. Considering the nature of turbulence, the observations reveal that, at a given point (or location) in the flow domain a distinguished pattern is repeated more or less regularly in time. Due to this fact, it is possible to extract the average values of the flow variables such as velocity and pressure in time and space. As the behavior of small scales (fluctuations) is not the subject of interest in some engineering applications, these small motions can be ignored over a range of specific time. Based on this assumption, Osborn Reynolds in 1895 suggested a decomposition based on mean and fluctuating parameters:

$$\phi = \bar{\phi} + \phi^{'} \tag{1.4}$$

where ϕ can be any quantity related to flow field, ("¯") identifies the mean (averaged) component and ("′") denotes the fluctuation part. Considering the time averaging for a given time T acting on a quantity ϕ yields:

$$\bar{\phi}(x,t) = \frac{1}{T}\int_{t}^{t+T} \phi(x,t)dt \tag{1.5}$$

Embedding this decomposition with the Navier-Stokes equations, the Reynolds equations for an incompressible Newtonian can be obtained as:

$$\frac{\partial \bar{u}_j}{\partial t} + \bar{u}_i \frac{\partial \bar{u}_j}{\partial x_i} = -\frac{1}{\rho}\frac{\partial \bar{p}}{\partial x_j} + \frac{\partial}{\partial x_i}\left(\nu \frac{\partial \bar{u}_j}{\partial x_i} - \overline{u_i^{'}u_j^{'}}\right) \tag{1.6}$$

The last term on the right hand side of Equation (1.6) is the Reynolds stress tensor. This term represents the effect of fluctuating components on the mean flow. In order to get a closed system of equations, the Reynolds stress tensor should be modeled. Boussinesq [5] developed a mathematical model for Reynolds stresses by defining the eddy-viscosity concept through an analogy between turbulence transport and the process of momentum transport via the molecular diffusion. In other words, the eddy-viscosity quantity (ν_t) connects the Reynolds stresses to the mean strain rate by:

$$\overline{u_i^{'}u_j^{'}} = -2\nu_t \bar{S}_{ij} + \frac{1}{3}\overline{u_k^{'}u_k^{'}}\delta_{ij} \tag{1.7}$$

To calculate the eddy viscosity term, a number of models have been introduced such as the Prandtl mixing model [6] and algebraic models of Baldwin-Lomax [7] and Cebeci-Smith [8]. One equation models are another alternative to model eddy viscosity through solving a transport equation for ν_t (Spalart-Allmaras [9]) or an undamped eddy viscosity ($R = \frac{k^2}{\epsilon}$)

(Rahman et al. [10]). Kolmogorov [11] developed the first "complete" model of turbulence since it needs no prior information on turbulence characteristics. Kolmogorov's k-ω model requires the solution of two differential equations for kinetic energy (k) and specific dissipation rate (ω). Subsequently, Wilcox [12] introduced some modifications and improvements to Kolmogorov's k-ω model. Another version of the two equation model was developed by Jones and Launder [13] known as the k-ϵ model. Apart from solving the k transport equation, this model also solves an equation for a dissipation rate ϵ. Launder and Sharma [14] developed a low-Reynolds version of the k-ϵ model. There are also other versions of the k-ϵ model (such as the model of Yakhot et al. [15]) but these are not within the scope of the current study.

1.2.3 Large Eddy Simulation (LES)

In the fluid flow, large eddies (or scales) are the main transporter of momentum and energy. In an LES the large structures of turbulence are resolved and the effect of small scales on the main flow can be modeled through the so-called subgrid-scale model (SGS) [16]. LES benefits from a decomposition similar to RANS in which the resolved and fluctuating components are separated through a "filtering" process:

$$u_i = \bar{u}_i + u_i' \tag{1.8}$$

The filtered part belongs to the resolved field and the fluctuating part is associated with the small eddies that are unresolved. The spatial filtering operation which is denoted as a bar $(\bar{.})$ can be expressed as:

$$\bar{u}(x,t) = \int G(y;x)u(x,y)dy \tag{1.9}$$

where G is a smoothing kernel acting in three dimensional space on the velocity (or pressure) field. The filter width Δ can be considered as a length scale which is not a fixed parameter. Applying the above filtering operation to instantaneous continuity and momentum equations, and considering the commutative properties, the resolved equation for an LES can be obtained as:

$$\frac{\partial \bar{u}_i}{\partial x_i} = 0 \tag{1.10}$$

$$\frac{\partial \bar{u}_i}{\partial t} + \frac{\partial \overline{u_i u_j}}{\partial x_j} = -\frac{1}{\rho}\frac{\partial \bar{p}}{\partial x_i} + \nu \frac{\partial^2 \bar{u}_i}{\partial x_j^2} \tag{1.11}$$

The non-linear term on the left-hand side of Equation (1.11) contains both the filtered and fluctuating components. The term $\overline{u_i u_j}$ can be decomposed and rewritten as:

$$\overline{u_i u_j} = \bar{u}_i \bar{u}_j + (\overline{u_i u_j} - \bar{u}_i \bar{u}_j) \tag{1.12}$$

The term in parentheses is called the SGS stress tensor τ_{ij}. Considering this fact, Equation (1.11) for an incompressible LES equation can be rewritten as:

$$\frac{\partial \bar{u}_i}{\partial t} + \frac{\partial \bar{u}_i \bar{u}_j}{\partial x_j} = -\frac{1}{\rho}\frac{\partial \bar{p}}{\partial x_i} + \nu \frac{\partial^2 \bar{u}_i}{\partial x_j^2} - \frac{\partial \tau_{ij}}{\partial x_j} \tag{1.13}$$

The SGS stress tensor is responsible for the effect of unresolved scales on the main flow field. Turbulence modeling in LES tries to offer a solution for this unknown term. The term τ_{ij} is typically replaced by an SGS model, accounting for the effects of small unresolved scales into the governing equations.

LES borrows its methodology from Kolmogorov's [11] self–similarity hypothesis that the large scales are dependent on the flow topology and properties which should be resolved separately for each flow case, while small scales represent universal characteristics that are common in many types of turbulent flows. The mechanism of LES in dealing with distinguished scales in turbulent flows enables it to provide a good compromise between DNS and RANS, since it does not need any heavy computational expenses of DNS; on the other hand, it produces more accurate results compared to the RANS. Nevertheless, one should be careful of not falling from an LES into the DNS because as the grid resolution in an LES increases, it tends to resolve all scales of turbulence exactly similar to the DNS.

The modeling of small (unresolved) eddies represents the core subject of LES turbulence modeling which was initiated by Smagorinsky [17] and continues up to this day. Since the introduction of the first SGS model by Smagorinsky [17], a few other SGS models have been proposed which are discussed in subsequent chapters. The current work also deals with the development and formulation of new SGS models.

2. Subgrid-Scale Modeling in LES

2.1 The Smagorinsky Model

LES can be divided into three distinguished categories or approaches in the context of sub-grid scale (SGS) modeling, namely, the eddy-viscosity model, similarity model and mixed model where the last one is a combination of the former two models. The main goal in all these three approaches is to provide and implement an effective model to account for the majority of unresolved scales in the turbulent flow. Eddy viscosity models are more popular than other available models in the LES. This model is based on the Boussinesq [5] assumption in bridging the turbulent and molecular transports through a so called turbulent or eddy-viscosity which is an artificial viscosity. Considering this fact, the SGS stress tensor can be defined as:

$$\tau_{ij} = -2\nu_t \bar{S}_{ij} + \frac{1}{3}\tau_{kk}\delta_{ij} \tag{2.1}$$

where ν_t represents the sub-grid scale eddy viscosity and $\bar{S}_{ij}$ is the resolved strain-rate tensor:

$$\bar{S}_{ij} = \frac{1}{2}\left(\frac{\partial \bar{u}_i}{\partial x_j} + \frac{\partial \bar{u}_j}{\partial x_i}\right) \tag{2.2}$$

The first SGS model or LES was proposed by Smagorinsky [17] based on the idea that the energy produced in resolved scales is equal to the energy dissipation on unresolved/small scales. The mechanism is such that the large eddies carrying the major fraction of turbulent energy transfers this energy to smaller scales. There is no doubt that physically, the viscous action is associated with the energy dissipation process. Since in an LES formulation the larger scales are resolved, it appears that the turbulent SGS stresses are smaller than their counterpart in RANS. The point is how much burden could be put on the SGS modeling that determines the key success to the LES. This aspect should be taken into account regardless of the energy transfer.

In the Smagorinsky model the turbulent eddy viscosity is related to the grid filter width and strain-rate:

$$\nu_t = (C_s\bar{\Delta})^2|\bar{S}| \tag{2.3}$$

where the velocity scale is proportional to the modulus of filtered strain rate tensor:

$$|\bar{S}| = \sqrt{2\bar{S}_{ij}\bar{S}_{ij}} \tag{2.4}$$

C_s is the Smagorinsky constant. The filter width Δ can be computed as the size of mesh spacing in the x-, y- and z- directions [18]:

$$\bar{\Delta} = (\Delta_x\Delta_y\Delta_z)^{\frac{1}{3}} \tag{2.5}$$

The Smagorinsky constant can be varied from one flow case to another flow case and also depends on the Reynolds number of the flow. Several studies reported that C_s can take different values ($0.05 < C_s < 0.5$) for different flow settings [18, 19, 20, 21].

In order to obtain the correct behavior close to the walls, a Van Driest type [22] damping function is introduced near the solid boundaries that accounts for the reduction of small fluctuations at those locations. This damping function is defined as:

$$\left(1 - \exp\left(\frac{-z^+}{25}\right)\right) \tag{2.6}$$

where z^+ is the dimensionless distance from the wall. Thus, the full eddy viscosity term in the Smagorinsky model takes the form:

$$\nu_t = \left[C_s\bar{\Delta}\left(1 - \exp\left(\frac{-z^+}{25}\right)\right)\right]^2|\bar{S}| \tag{2.7}$$

The Smagorinsky model is a popular SGS model due to its simplicity, robustness and its ability to reproduce the global energy flux from the resolved to small scales [23]. However, it suffers from a few shortcomings, firstly because of the Smagorinsky constant in the viscosity term, requiring a priori information on the flow topology (which varies for different flow problems). This issue can create an excessive dissipation in certain types of flow. Another issue is that it needs an *ad-hoc* wall damping near the solid walls to correct the near-wall behavior of the model [24].

2.2 The dynamic Smagorinsky model (DSM)

Germano et al. [25] proposed a modified version of the Smagorinsky model (SM) in which the constant C_s is computed dynamically varying in time and space. Like the SM, the DSM also benefits from the Boussinesq [5] approximation for the stress tensor term. In order to dynamically compute the eddy viscosity term, the DSM applies (along with the grid filter) an additional explicit secondary filter called the "test filter". The grid scale of this test-filter is denoted by $\tilde{\Delta} = \alpha\bar{\Delta}$; the test-filter width $\tilde{\Delta}$ must be greater than the grid-filter width $\bar{\Delta}$, i.e., $\alpha > 1$. Applying the test filter result in the Germano identity requiring:

$$L_{ij} = T_{ij} - \tilde{\tau_{ij}} = \widetilde{\overline{u_i u_j}} - \tilde{\bar{u}}_i \tilde{\bar{u}}_j - \left(\widetilde{\overline{u_i u_j}} - \widetilde{\bar{u}_i \bar{u}_j} \right) = \widetilde{\bar{u}_i \bar{u}_j} - \tilde{\bar{u}}_i \tilde{\bar{u}}_j \tag{2.8}$$

where T_{ij} is the SGS stress on the test–filter level. The stress components L_{ij} can be interpreted as the stress associated with the smallest resolved scales between the test–filter scale ($\tilde{\Delta}$) and the grid–filter scale ($\bar{\Delta}$). The stress tensor L_{ij} is called the Leonard stress and can be directly computed from the resolved scales.

If $\bar{C}_s$ is assumed not to change significantly from the grid–filter to the test–filter scales, the error generated by using the Smagorinsky model in the Germano identity is:

$$E_{ij} = L_{ij} - \frac{\delta_{ij}}{3} L_{kk} - \bar{C}_s M_{ij}, \qquad M_{ij} = 2\bar{\Delta}^2 \left(\widetilde{|\bar{S}|\bar{S}_{ij}} - \alpha^2 \eta |\tilde{\bar{S}}| \tilde{\bar{S}}_{ij} \right) \tag{2.9}$$

with $\eta = \tilde{C}_s/\bar{C}_s$. Generally $\alpha = 2$ and the scale variance ($\eta = 1$) is assumed. Following Lilly's idea [26], the model coefficient $\bar{C}_s$ is obtained by seeking a value for $\bar{C}_s$ which minimizes the square of the error E^2. Therefore, taking $\partial E^2 / \partial \bar{C}_s$ and setting it to zero gives

$$\bar{C}_s = \frac{L_{ij}\, M_{ij}}{M_{ij}\, M_{ij}} \tag{2.10}$$

The model coefficient $\bar{C}_s$, thus obtained is a local quantity, varying in time and space in a fairly wide range having positive and negative values. Although a negative $\bar{C}_s$ (and therefore a negative ν_T) is often interpreted as the flow of energy from the sub–grid scale eddies to the resolved eddies (referred to as "back–scatter") and regarded as a desirable attribute of the dynamic model; too large a negative ν_T causes numerical instability, which lead to divergence of the numerical solution. To avoid this, $\bar{C}_s$ is simply clipped at zero.

2.3 Wall-Adapting Local Eddy-Viscosity (WALE) model

The WALE model is devised by Nicoud and Ducros [27] based on the square of the velocity gradient tensor; the spatial operator $\overline{OP} = (S^d_{ij}S^d_{ij})$ consists of a mixing of both the local strain and rotation rates. Unlike the Smagorinsky model, this model accounts for both strain and rotational rate. Thus, all the turbulence structures relevant for the kinetic energy dissipation are detected by the model; the eddy-viscosity goes naturally to zero in the vicinity of a wall so that neither (dynamic) constant adjustment nor damping function is required to compute wall bounded flows. The model produces a zero eddy viscosity in the case of a pure shear. Thus, it is possible to reproduce the laminar to turbulent transition process through the growth of linear unstable modes. The eddy-viscosity in the Wale model is obtained from:

$$\nu_t = (C_w\Delta)^2 \frac{(S^d_{ij}S^d_{ij})^{\frac{3}{2}}}{(\bar{S}_{ij}\bar{S}_{ij})^{\frac{5}{2}} + (S^d_{ij}S^d_{ij})^{\frac{5}{4}}} \qquad (2.11)$$

Where S^d_{ij} is traceless symmetric part of the square of the velocity gradient tensor:

$$S^d_{ij} = \frac{1}{2}(\bar{g}_{ik}\bar{g}_{kj} + \bar{g}_{jk}\bar{g}_{ki}) - \frac{1}{3}\delta_{ij}(\bar{g}_{kk})^2 \qquad (2.12)$$

where $\bar{g}_{ij}$ denotes the velocity gradient tensor. Like the Smagorinsky constant C_s, C_w can take different values depending on the nature of the flows, but the C_w values are usually between 0.3 and 0.6.

2.4 Vreman model

Vreman [28] devised an SGS model in 2004. The turbulent viscosity in the Vreman model is defined as:

$$\nu_t = C_V \sqrt{\frac{\beta_{\bar{\beta}}}{\bar{\alpha}_{ij}\bar{\alpha}_{ij}}} \qquad (2.13)$$

where $\bar{\alpha}_{ij}$ indicates the derivatives of the filtered velocity $\bar{u}$

$$\bar{\alpha}_{ij} = \frac{\partial \bar{u}_j}{\partial x_i} \qquad (2.14)$$

Tensor β is related to the gradient model [29, 30] in its general anisotropic form and it is positive semidefinite ($\beta_{\bar{\beta}} \geq 0$). $\beta_{\bar{\beta}}$ is an invariant of the matrix β:

$$\beta_{\bar{\beta}} = \bar{\beta}_{11}\bar{\beta}_{22} + \bar{\beta}_{11}\bar{\beta}_{33} + \bar{\beta}_{22}\bar{\beta}_{33} - \bar{\beta}^2_{12} - \bar{\beta}^2_{13} - \bar{\beta}^2_{23}, \qquad \bar{\beta}_{ij} = \Delta^2_m\bar{\alpha}_{mi}\bar{\alpha}_{mj} \qquad (2.15)$$

In Equation (2.13), C_V is the model constant and is related to the Smagorinsky constant with approximately $C_V = 2.5C_s$ for an isotropic turbulence. Δ_m is the grid filter width. The Vreman model satisfies the realizability conditions and it requires a single filter (grid filter) and the first-order derivatives of the velocity field.

2.5 Scale-similarity model

Scale-similarity or similarity models are based on the assumption that flow fields at scales of consecutive sizes have some similarity. This means that the Leonard stress, L_{ij} produced by filtering at the test-filter level plays as a principal model for the SGS stress which is the result of filtering at the grid-filter level. The idea of the scale-similarity model was introduced by Bardina et al. [20]. Scale-similarity models consist of the non–eddy viscosity category of SGS models (which are not the scope of the current work). The main purpose of these models is to account for the unresolved scales of turbulence through the inclusion of an additional filtering process on the velocity field and their derivatives. The mechanism of similarity models works in such a way as to capture the similarities associated with stresses on neighboring velocity scales, especially those that are above and below the LES cutoff length. Although showing an acceptable agreement with available experimental data, this model has limited application in practical LES since it underestimates the energy cascade, which causes causing an underestimation of the subgrid dissipation. One way to overcome this limitation is to combine a scale similarity model with a subgrid viscosity model resulting in so called mixed model. One example can be by mixing a scale similarity model with a Germano-Lilly one in which the respective weights of the scale-similarity and SGS eddy-viscosity parts of the model can be modified. This mixed model allows a better control of the dissipation by inclusion of an eddy-viscosity term.

3. Mathematical Formulation for the Proposed Models

3.1 Zero–equation Model

In this section, the underlying mechanism of a zero-equation model is discussed. A comprehensive presentation of this model can be found in Publications I and III. This model is called RAST (Rahman-Agarwal-Siikonen-Taghinia). It is also worthwhile mentioning that the authors also devised an RANS model called RAS (Rahman-Agarwal-Siikonen) from which the model now presented has taken its name.

Applying the spatial filter to incompressible Navier-Stokes equations and using the commutation characteristics, the LES equations yield:

$$\frac{\partial \bar{u_j}}{\partial x_i} = 0 \tag{3.1}$$

$$\frac{\partial \bar{u}_i}{\partial t} + \frac{\partial \bar{u}_i \bar{u}_j}{\partial x_j} = -\frac{1}{\rho}\frac{\partial \bar{p}}{\partial x_i} + \frac{\partial}{\partial x_j}\left(\nu \frac{\partial \bar{u}_i}{\partial x_j}\right) - \frac{\partial \tau_{ij}}{\partial x_j} \tag{3.2}$$

where the overbar $(\bar{.})$ denotes the application of grid filter and ν is the kinematic viscosity. On the right–hand side, an unresolved term τ_{ij} remains to be modeled. This term is analogous to the Reynolds–stress tensor of RANS turbulence modeling. Since in the LES formulation the larger length scales are resolved, it denotes the turbulent SGS stresses and hence, is smaller than its counterpart in RANS. The SGS stress tensor is defined as

$$\tau_{ij} = \overline{u_i u_j} - \bar{u}_i \bar{u}_j \tag{3.3}$$

The role of the SGS model is to remove energy from the resolved scales. In an LES, the small dissipative scales need to be modeled. Therefore, the SGS model is employed to account for the dissipation of turbulent kinetic energy to heat. Thus, the SGS models do not attempt at producing SGS stresses accurately but only account for their effect in a statistical sense.

The unknown SGS turbulent stresses resulting from the filtering operation in Equation (3.3) need a closure. Following the Boussinesq approximation, the relationship between the anisotropic part of the SGS stress tensor and the resolved strain–rate tensor can be expressed as:

$$\tau_{ij} - \frac{1}{3}\tau_{kk}\,\delta_{ij} = \tau_{ij} - \frac{2}{3}k_{sgs}\,\delta_{ij} = -2\nu_T\bar{S}_{ij}, \qquad \bar{S}_{ij} = \frac{1}{2}\left(\frac{\partial \bar{u}_i}{\partial x_j} + \frac{\partial \bar{u}_j}{\partial x_i}\right) \tag{3.4}$$

where k_{sgs} is the SGS kinetic energy. The isotropic part of stress tensor $(\frac{2}{3}k_{sgs}\delta_{ij})$ is implicitly added to the pressure. The SGS eddy–viscosity ν_T is assumed to be a scalar quantity and is determined as:

$$\nu_T = C_\mu\,\bar{\Delta}^2\,\bar{S} \tag{3.5}$$

where C_μ is a model coefficient, $\bar{S} = \sqrt{2\bar{S}_{ij}\bar{S}_{ij}}$ is the invariant of resolved strain–rate tensor, and $\bar{\Delta}$ is the grid–filter length (or width) computed from the cell–volume [18]:

$$\bar{\Delta} = (\Delta_1\Delta_2\Delta_3)^{\frac{1}{3}} \tag{3.6}$$

where Δ_1, Δ_2 and Δ_3 are the grid sizes in x-, y- and z- directions, respectively.

The eddy–viscosity coefficient C_μ appearing in Equation (3.5) is an indisputably flow–dependent quantity which can be computed based on the resolved strain–rate $\bar{S}_{ij}$ and vorticity $\overline{W}_{ij}$ tensors in question (which is extensively discussed in section 3.1.1). The resolved strain–rate tensor $\bar{S}_{ij}$ is given in Equation (3.4). The resolved vorticity $\overline{W}_{ij}$ is given by

$$\overline{W}_{ij} = \frac{1}{2}\left(\frac{\partial \bar{u}_i}{\partial x_j} - \frac{\partial \bar{u}_j}{\partial x_i}\right) \tag{3.7}$$

The invariant of resolved vorticity tensor is defined by $\overline{W} = \sqrt{2\overline{W}_{ij}\overline{W}_{ij}}$. In the current study, C_μ is evaluated in a manner analogous to that employed in the RANS modeling [31]. In particular, the SGS turbulent kinetic energy k_{sgs} transport model accounts for the history and non–local effects, having the potential to benefit complex flows with non–equilibrium turbulence [32]. The SGS kinetic energy is defined as:

$$k_{sgs} = \frac{1}{2}\tau_{kk} = \frac{1}{2}\left(\overline{u_k u_k} - \bar{u}_k\bar{u}_k\right) \tag{3.8}$$

which can be obtained by contracting the sub–grid scale stress in Equation (3.3). However, with the current zero–equation model k_{sgs} is computed algebraically as follows. Assuming the SGS dissipation ϵ_{sgs} would exactly balance the scaling of the SGS production of k_{sgs} yields [24]:

$$\epsilon_{sgs} = \frac{k_{sgs}^{\frac{3}{2}}}{\bar{\Delta}} = 2\nu_T\bar{S}_{ij}\bar{S}_{ij} = \nu_T\bar{S}^2 \tag{3.9}$$

Alternatively, the underlying assumption is the local equilibrium between the transferred energy through the grid–filter scale and the dissipation of kinetic energy at small sub–grid scales. Considering Equations (3.5) and (3.9) k_{sgs} can be obtained as:

$$k_{sgs} = C_\mu^{\frac{2}{3}} (\bar{\Delta}\bar{S})^2 \tag{3.10}$$

The Yoshizawa–relation [33] for k_{sgs} is similar to the one given in Equation (3.10). Nevertheless, the difference is distinguishable in the sense that the former introduces a constant coefficient with the formulation. The variable coefficient C_μ in Equation (3.10) depends non–linearly on both the resolved strain–rate and vorticity parameters, and it allows k_{sgs} for an intrinsic ability to adapt to the local level of turbulent activity to some extent.

3.1.1 Eddy–viscosity coefficient C_μ

The requirement of realizability in a turbulence model is of utmost importance. The realizability concepts to SGS stress components are:

$$\tau_{ii} \geq 0 \tag{3.11}$$

with no summation over i and,

$$\frac{{\tau_{ij}}^2}{\tau_{ii}\tau_{jj}} \leq 1 \tag{3.12}$$

with no summation on i and j.

The realizability conditions represent the mathematical requirement to prevent a turbulence model from producing nonphysical results [34]. The commonly used isotropic eddy–viscosity model with a constant C_μ becomes unrealizable in the case of a large strain–rate producing negative normal stresses and thus the realizability is violated [34]. The realizability principle applied to the present model, i.e., Equations (3.4), (3.5) and (3.10) implies that

$$\frac{\tau_{ii}}{2k_{sgs}} = \frac{1}{3} - C_\mu^{\frac{1}{3}} \frac{\bar{S}_{ii}}{\bar{S}} \geq 0 \tag{3.13}$$

Note that each SGS normal-stress component should satisfy the realizability condition and hence Eq. 3.13 must be taken without the summation over i. From equation (3.13), it can be noted that the negative normal stresses can occur, e.g., when $\bar{S}_{ii}/\bar{S} > 0.5$ with $C_\mu = 0.3$. To ensure realizability, the model coefficient C_μ cannot be a constant (however, even variable eddy viscosity coefficient does not necessarily guarantee the realizability criteria in all grid cells). It must be related with the resolved flow deformation rate. Accordingly, a plausible formulation for C_μ as suggested by Rahman and Siikonen [31] in an RANS modeling is adapted here:

$$C_\mu = \frac{1}{2\left(1 + T_t \bar{S}\sqrt{1+\Re^2}\right)} \tag{3.14}$$

where T_t is the hybrid time scale and $\Re = \overline{W}/\bar{S}$ is a dimensionless parameter which is very useful in characterizing the flow. For instance, for a pure shear flow $\Re = 1$, whereas for a plane strain flow $\Re = 0$. It is important to emphasize here that C_μ should be appropriate for both the shear and vorticity dominated flows that are far from equilibrium. A detailed analysis of the model realizability is available in References [31, 35, 36].

The total turbulent normal stress profiles obtained after adding up the resolved and unresolved parts of the Reynolds stresses benefit from Equation (3.13) when compared with the DNS and experimental data, especially in the near–wall region. In particular, Equation (3.13) shows that the energy components are always positive due to the inclusion of coefficient C_μ, a simple variant to the general non–linear eddy–viscosity model discussed by Pope [21].

It should be emphasized that the new formulation usually produces realizable SGS stresses but it obviously does not guarantee realizability everywhere in the computational domain. This shortcoming is probably related to the fact that the new model uses the Boussinesq (linear/isotropic) approximation for the SGS Reynolds stresses. However, the realizability constraints are not so important for the SGS modeling. To this end, it can be stressed that applying a variable eddy-viscosity coefficient is better than that of a constant one (which is a common practice for LES modeling).

A plot of C_μ against the DNS data [38] for a fully developed turbulent channel flow with $Re_\tau = 395$ is shown in Figure 3.1 which is obtained from LES calculation. A good agreement with the data is obtained. This demonstrates that the model can be integrated all the way down to the wall without adding a damping function to the eddy–viscosity. The strain–dependent coefficient C_μ in the eddy–viscosity equation provides natural damping as the wall is approached. This feature is of significant importance in the problem with flow separation and reattachment. It seems likely that C_μ may converge to a higher value of 0.5 as the shear parameter $(T_t\bar{S}) \to 0$. In general, C_μ is highly flow–dependent and several authors [39, 40, 41] have suggested a wide range of 0.0–0.6. To this end, it can be stressed that the WALE [27] and the Vreman models [28], in particular, retain the eddy–viscosity approach and modify the Smagorinsky model to allow for an adaptation of its structure to the flow. Their modification of the model coefficient C_μ is similar to the one proposed in the current model. Nevertheless, the glaring difference is that the WALE and the Vreman models additionally invoke flow–dependent constants with C_μ in contrast to the present model.

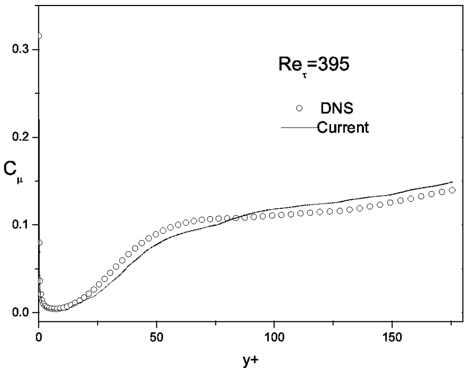

Figure 3.1. C_μ profile against DNS data

3.1.2 Hybrid time scale T_t

The flow shows strong inhomogeneity and anisotropy in the viscous layer with $y^+ < 5$ and, therefore, the use of the dynamics time scale k/ϵ is not appropriate in that region. In the present study, the total kinetic energy k and the dissipation ϵ are determined by the expressions:

$$k = k_{sgs} + \frac{1}{2}\bar{u}'_k\bar{u}'_k, \qquad \epsilon = 2\left(\nu + \nu_T\right)\bar{S}_{ij}\bar{S}_{ij} \tag{3.15}$$

The average of instantaneous resolved velocity $\bar{u}_i$ is collected continuously as

$$< \bar{u}_i >_m = [(m-1) < \bar{u}_i >_{m-1} + (\bar{u}_i)_m]/m \tag{3.16}$$

where m is the number of instants in the average. The averaged values of Reynolds stresses are recorded in a similar manner:

$$(\bar{u}'_i)_m = (\bar{u}_i)_m - < \bar{u}_i >_m \tag{3.17}$$

$$(\bar{u}'_i\bar{u}'_j)_m = \Big[(m-1)(\bar{u}'_i\bar{u}'_j)_{m-1} + \{(\bar{u}_i)_m - < \bar{u}_i >_m\}\{(\bar{u}_j)_m - < \bar{u}_j >_m\}\Big]/m \tag{3.18}$$

where m is the number of instants in the average. From Equation (3.18) the resolved turbulent kinetic energy $\left(\frac{1}{2}\bar{u}'_k\bar{u}'_k\right)$ in Equation (3.15) can be calculated easily. It is worth mentioning that in the case of a transient inhomogeneous flow, it is problematic to apply the above-mentioned approach to calculating the resolved kinetic energy, and the definitions of the current equations are valid only for statistically steady flows. However, if the transient is slow enough, a good approximation can be achieved. Equations (3.15)-(3.18) are applied to an indoor airflow problem [42] to obtain the resolved turbulent kinetic energy which can be considered as an inhomogeneous transient flow case having no homogeneous direction. According to the above discussion and low Reynolds number of the current cases in this thesis, all simulations share a good agreement with the experimental data available.

The total dissipation rate ϵ is evaluated as follows:

$$\epsilon = \nu \overline{\frac{\partial u_i}{\partial x_j}\frac{\partial u_i}{\partial x_j}} \tag{3.19}$$

which is referred to as filtered dissipation. We can either try to model ϵ directly or combine it with the resolved dissipation and model the difference:

$$\epsilon_{sgs} = \nu\left(\overline{\frac{\partial u_i}{\partial x_j}\frac{\partial u_i}{\partial x_j}} - \frac{\partial \bar{u}_i}{\partial x_j}\frac{\partial \bar{u}_i}{\partial x_j}\right) = 2\nu\left(\overline{S_{ij}S_{ij}} - \bar{S}_{ij}\bar{S}_{ij}\right) \tag{3.20}$$

which can be called as the SGS energy dissipation. The above-mentioned expression can be recast as:

$$2\nu\overline{S_{ij}S_{ij}} = 2\nu\bar{S}_{ij}\bar{S}_{ij} + \epsilon_{sgs} = 2\left(\nu + \nu_T\right)\bar{S}_{ij}\bar{S}_{ij} = \epsilon \tag{3.21}$$

Employing k/ϵ for the dynamic time scale results in the time scale vanishing when approaching a wall, where $k \to 0$ and ϵ is non–zero. To avoid this, the Kolmogorov time scale $\sqrt{\nu/\epsilon}$ is used as a lower bound close to the wall, where the viscous dissipation is dominant. To interpolate smoothly between the Kolmogorov and dynamic time scales, a hybrid time scale is formed as

$$T_t = \sqrt{\frac{k^2}{\epsilon^2} + C_T^2\,\frac{\nu}{\epsilon}} = \frac{k}{\epsilon}\sqrt{1 + \frac{C_T^2}{Re_T}}, \qquad Re_T = \frac{k^2}{\nu\,\epsilon} \tag{3.22}$$

where Re_T is the turbulence Reynolds number. Equation (3.22) guarantees that the eddy time scale never falls below the Kolmogorov time scale $C_T\sqrt{\nu/\epsilon}$, which is dominant in the immediate neighborhood of the solid wall. Alternatively, the turbulence time scale is k/ϵ at a large Re_T but approaches the Kolmogorov limit $C_T\sqrt{\nu/\epsilon}$ for $Re_T \ll 1$. The empirical constant $C_T = \sqrt{2}$ associated with the Kolmogorov time scale is estimated from the behavior of the k–transport equation in the RANS modeling as given in Reference [35]. In the viscous sublayer $k = y^2/(C_T^2 \nu/\epsilon)$, where the basic scale is the Kolmogorov time scale and y is the normal distance from the wall. Besides, the k-equation reduces to $\nu \partial^2 k/\partial y^2 = \epsilon$ as the wall is approached. Combining these two relations gives $C_T = \sqrt{2} \approx 1.42$, which is close to the experimental value of about 1.5 [43].

3.2 One–equation Model

The concept behind the one–equation model is similar to that of the zero–equation model. Although there is one difference in the representation of the kinetic energy calculation and also a minor change in the form of the turbulent eddy viscosity, it can be regarded as a modified version of a zero-equation model.

Both the original and dynamic Smagorinsky models are essentially algebraic models in which the SGS stresses are obtained as a function of the resolved velocity scales. The underlying assumption is that there is a local equilibrium between the transferred kinetic energy through the grid–filter scale and the dissipation of kinetic energy at small sub–grid scales. The SGS turbulence is thus represented more faithfully by accounting for the transport of SGS kinetic energy. The transport of SGS turbulent kinetic energy can account for the history and non–local effects, which potentially benefits complex flows with non–equilibrium turbulence. The transport equation for k_{sgs} is given by [19, 32, 41]:

$$\frac{Dk_{sgs}}{Dt} = \nabla[(\nu + \nu_T)\nabla k_{sgs}] + P_{k_{sgs}} - C_\epsilon \frac{k_{sgs}^{\frac{3}{2}}}{\bar{\Delta}} \tag{3.23}$$

where the production term $P_{k_{sgs}}$ is computed from

$$P_{k_{sgs}} = -\tau_{ij} \frac{\partial \bar{u}_i}{\partial x_j} \tag{3.24}$$

The turbulent eddy viscosity is calculated based on k_{sgs} as:

$$\nu_t = C_\mu \bar{\Delta} \sqrt{k_{sgs}} \tag{3.25}$$

The constant–coefficient models suggest a value of 1–1.5 for the dissipation term coefficient C_ϵ [44], which falls within the range given by the dynamic model [32] for turbulent channel flow computations. Therefore, $C_\epsilon = 1.05$ is set and reference computations show that the current LES yields predictions in good agreement with the direct numerical simulation (DNS) and experimental data. Noteworthily, the difference between the current and previous one–equation SGS models [19, 41] is that Equation (3.23) contains a variable eddy–viscosity coefficient, which provides a better solution than the common approaches in LES. A detailed discussion of the model can be found in Publication II where the results obtained for various fluid flow cases are presented and discussed.

4. Numerical test cases

4.1 Turbulent channel flow

In this section, the prediction of one–equation model for a turbulent channel flow is presented and discussed briefly. The turbulent channel flow serves as a suitable benchmark in testing new turbulence models due to its simplicity and importance. The computational settings and schemes are extensively discussed in Publication II. The results and a detailed analysis of the diffuser flow- which is a significant adverse-pressure gradient case can also be found in Publication II.

The large eddy simulation is performed for turbulent channel flows at $Re_\tau = 180$ and $Re_\tau = 395$ based on the wall friction velocity u_τ and half-height channel δ. A uniform grid spacing is used in both the stream–wise and span–wise directions. The grid is stretched in the wall–normal direction. A summary of the grid distributions is given in Table 4.1. It should be mentioned that the current domain dimensions and grid distribution have been used in previous studies [45, 48] and their results showed that increasing the domain width does not affect the final results for the case with Re =395. A second-order upwind scheme for convective terms and a central differencing scheme for diffusion terms are applied. It is well known that the second-order upwind scheme can be too dissipative in some cases. However, it is more stable and converges faster than the central-scheme (which can produce dispersive errors) and does not need any artificial dissipation for its stabilization. Since the current simulations yielded good results using the second-order upwind scheme, especially at a lower Reynolds number where there is a main flow direction, it has been applied in the present study.

Figure 4.1 shows the mean velocity profiles for different models. Predictions of the present model are comparable/superior to those obtained with the DSM. In the mean velocity profile the upward shift in the log–layer is a little bit smaller than that of the DSM. The turbulent eddy viscosity profiles in Figure 4.5 show that the eddy–viscosities are under-predicted at $y^+ > 30$, explaining the overprediction of both the models at a dimensionless wall–distance larger than about 30. However, taking into account that the numerical method is only second–order accurate, there is reasonable agreement with the DNS data. Profiles of total turbulent shear stresses are displayed in Figure 4.2. Agreement of both the model predictions with the DNS data is fairly good. It seems likely that the present model returns superior predictions relative to the DSM.

Figure 4.3 shows the RMS values of the resolved velocity fluctuations. The stream–wise RMS velocities are over–predicted by both models; this is probably a consequence of the over–prediction of stream–wise mean velocities shown in Figure 4.1. Near the wall both the SGS models are in good agreement with the DNS. The wall–normal and span–wise RMS values are fairly accurate. Nevertheless, the current model is slightly better than the DSM model in predicting the turbulence statistics provided by the DNS.

Further examination of the model performance is directed to the total k^+ (resolved+modeled) profiles as illustrated in Figure 4.4. As is evident, k^+ closely matches the unfiltered DNS data. This approach is usually followed in the literature (i.e., to compare unfiltered DNS or experimental data with the sum of the resolved and unresolved/modeled part of the Reynolds stress tensor).

Table 4.1. Grid parameters for LES of a turbulent channel flow. L_x, L_y, L_z are stream–wise, wall–normal and span–wise lengths, respectively. δ is the channel half-height, $N_{x,y,z}$ and $\Delta(x,y,z)^+$ are the number of grid points and resolution in wall units, respectively.

Re_τ	L_x	L_y	L_z	N_x	N_y	N_z	Δx^+	$\Delta y^+(min-max)$	Δz^+
180	12δ	2δ	4δ	48	48	48	55	0.5–16	25
395	6δ	2δ	2δ	64	64	64	45	0.9–34	20

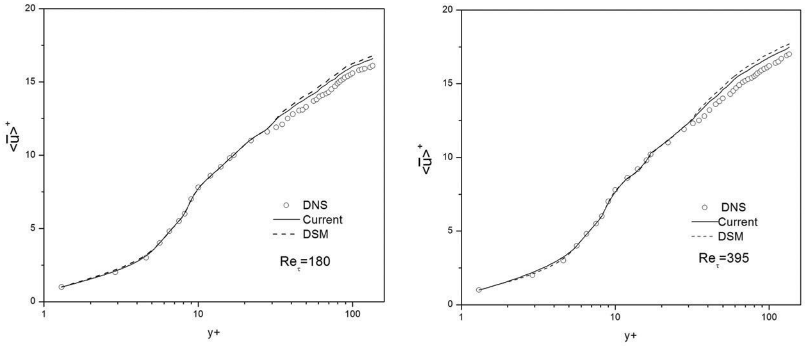

Figure 4.1. Channel flow predictions compared with DNS results

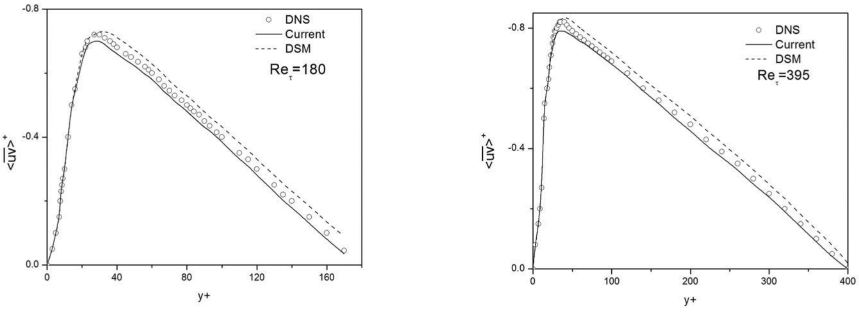

Figure 4.2. Total shear stress profiles for channel flow

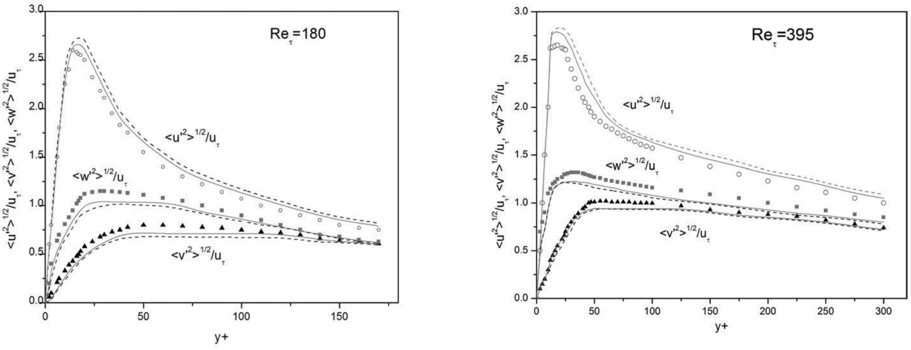

Figure 4.3. RMS values of fluctuating resolved velocity components for channel flow: current model (solid lines); DSM (dashed lines) and DNS (symbols)

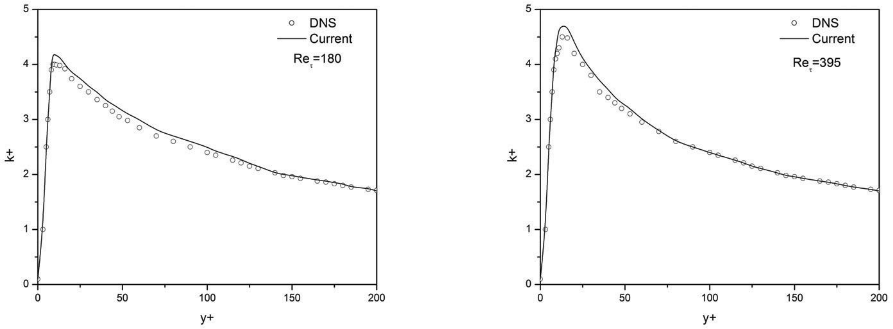

Figure 4.4. Total kinetic energy comparison with DNS results

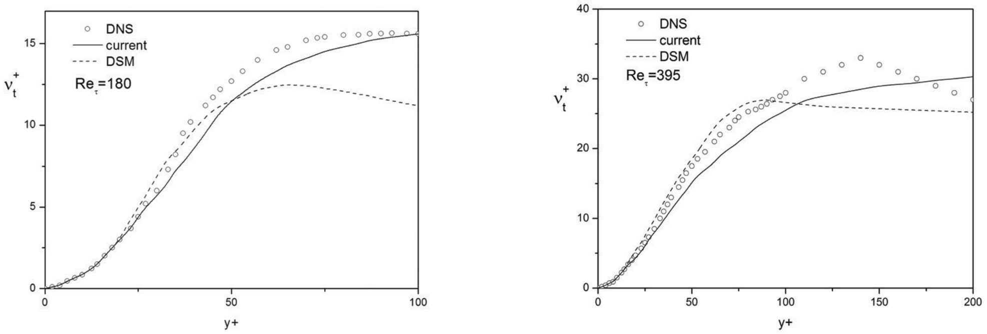

Figure 4.5. Eddy viscosity distribution for channel flow

4.2 Indoor airflow

The performance of the RAST zero-equation model is investigated for indoor airflow in different ventilation scenarios. A detailed discussion of this study is extensively presented in Publication IV where the results for mixed and forced convection, and an impinging jet in a room are demonstrated. Therefore, in this section, the results for forced convection are discussed.

The computational domain follows the experimental work of Nielsen et al. [49] as shown in Fig. 4.6. For a better assessment, the predictions from the SST-SAS model are also included.

A second–order upwind flux–difference splitting scheme for convective terms and a central differencing scheme for diffusion terms are applied. For time integration, a Crank–Nicolson second-order accurate scheme is utilized. It should be mentioned that commutation errors on non-uniform grids are well-known problems, however they are usually neglected in practice. In order to control this issue all computations are performed using the top–hat filter (second–order filter) which is positively defined in the physical space. A grid stretching of 1.05 is used in the wall-normal and stream-wise (only for the diffuser and hill flow cases) directions, but the grid distributions in the stream-wise and span-wise directions are uniform. Second-order accurate numerical schemes are used so that the commutation errors are of the order of the truncation error. However, when using a higher-order spatial discretization scheme, the order of the filter will dictate the order of accuracy in the solution [50].

The flow geometry is three dimensional. The inlet slot-height $h_{in}/H = 0.056$ and outlet slot-height $h_{out}/H = 0.16$. The slot-width of the inlet and the outlet is the same as the model width. The Reynolds number is $Re = U_{in}h_{in}/\nu = 5 \times 10^3$ based on the inlet slot-height. Apart from the inlet and the outlet, all other boundaries are defined as walls.

The mean velocity and fluctuation profiles at horizontal $y/H(= 0.028, 0.972)$ and vertical $x/H(= 1, 2)$ locations are demonstrated in Figures 4.7 and 4.8, respectively. As shown in Figure 4.7, the predictions of both models agree well with the experimental data. However, the RAST model shows a better agreement with measurements as the flow travels away from the inlet. Considering the mean velocity distribution at $x/H = 1$ and $x/H = 2$, the RAST model predictions agree very well with the experimental data close to the wall region (with less than 3% error) due to its sensitivity to the recirculation and streamline curvature. On the other hand, the turbulent eddy viscosity of the SST-SAS model is under–predicted close to the top wall (the jet region) causing an over–prediction of the mean velocity in that location. Overall, the trend and magnitude of the predicted velocities are almost the same for both models, although the RAST model shows a better performance close to the top and bottom walls.

Figure 4.8 shows the root–mean–square (RMS) velocity fluctuation values for the RAST and SST-SAS models. A lower turbulent fluctuation at $y/h = 0.972$ and $y/h = 0.028$ is due to the under–estimation of the turbulent eddy–viscosity in the SST-SAS model which can explain the discrepancies between the computed results and measured data of the mean velocity close to the wall at these locations. The predictions of both models are consistent with the experimental data at $x/H = 1$ and $x/H = 2$ with a maximum deviation of 5%, however, the RAST model gives more accurate results in terms of turbulence statistics.

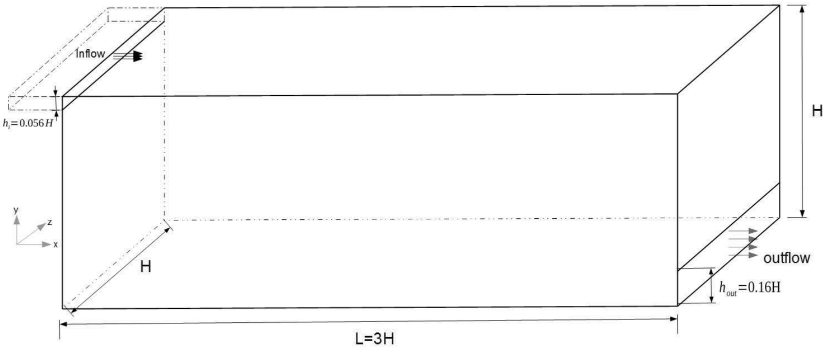

Figure 4.6. Computational domain for forced convection case.

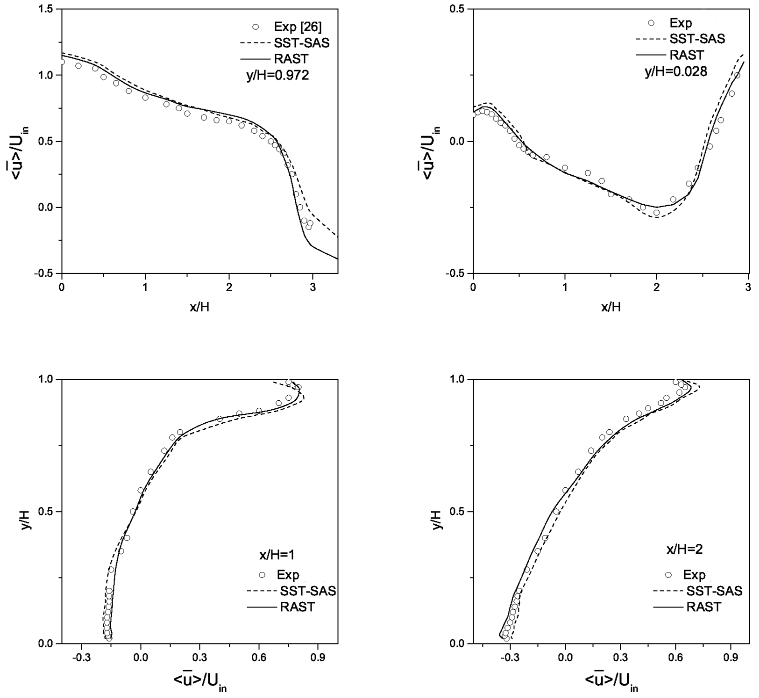

Figure 4.7. Predicted mean velocity profiles at different locations for forced convection

.

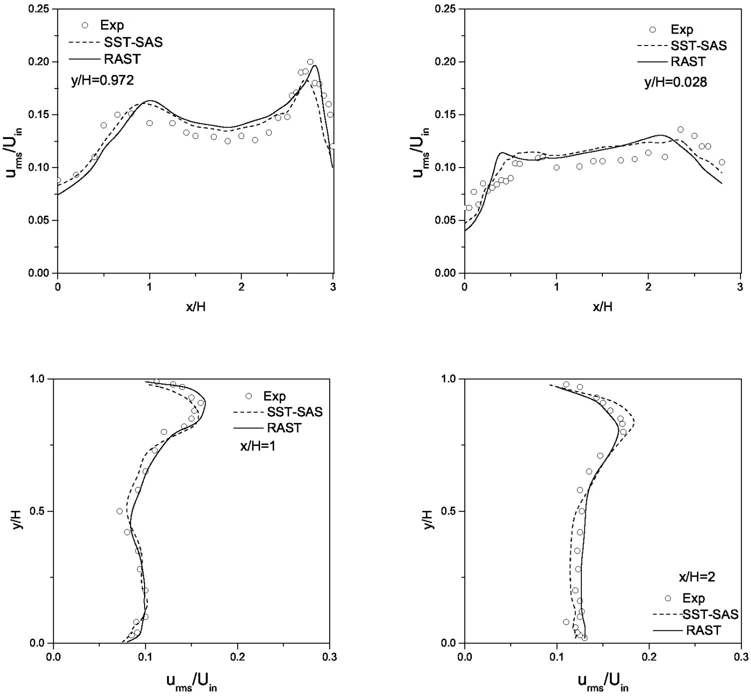

Figure 4.8. Predicted RMS fluctuating velocity profiles at different locations for forced convection

4.3 Flow past a circular cylinder

The flow over a circular cylinder is a significant phenomenon encountered in a wide range of engineering and industrial applications.The general characteristics of the flow past bluff bodies include a laminar separation, a reattachment and vortical motions. This section deals with assessing the performance of the RAST (Rahman–Agarwal–Siikonen–Taghinia) model in predicting the flow features around a circular cylinder at $Re_D = 3900$. The results are compared with available experimental data and with those obtained by the dynamic Smagorinsky model (DSM). An extensive discussion on this case and flow features can be found in Publication V.

The computational domain with the origin at the center of the cylinder is illustrated in Figure 4.9. The geometry follows the work of Franke and Frank [51]. The stream–wise direction is along the x–axis with $x = 0$ at the center of the cylinder, the y–axis is the vertical axis with $y = 0$ being the wake center-line, and the z–axis is the span–wise direction with $z = 0$ being the center-line of cylinder. The mean stream–wise velocity $\bar{u}$ along the centerline with the experimental data of Lourenco and Shih [52] is illustrated in Figure 4.10. On the wake centerline $\bar{u}$ is zero at the base of the cylinder (no–slip condition); it reaches a negative maximum U_{min} in the recirculation zone and converges asymptotically and monotonously toward the external velocity U_∞. As can be seen, the DSM under–estimates the U_{min} velocity at the very near wake region causing a shorter recirculation zone while the RAST model results agree fairly well with the experimental data. This may be due to the over–estimation of

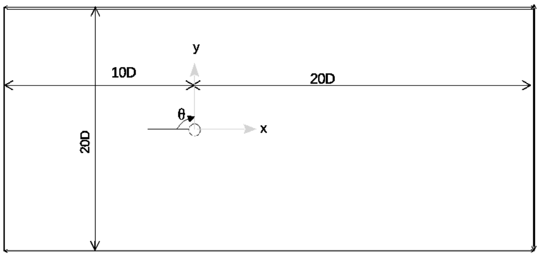

Figure 4.9. Computational domain for the circular cylinder

turbulent eddy–viscosity by the DSM. The sensitivity of C_μ to the flow with recirculation and reattachment, associated with the RAST model is obviously ascertained at this sub–critical flow. In fact, the quality of recirculation–length L_r prediction is the deciding factor about the agreement between experimental and numerical statistics. L_r corresponds to the distance between the base of cylinder and the change in sign of $\bar{u}$. The stream–wise recirculation lengths predicted by the DSM and RAST model are $L_r/D = 1.3$ and $L_r/D = 1.35$, respectively. The experimental value [52, 53] of recirculation length $L_r/D = 1.33 \pm 0.2$, which is in the range predicted by the RAST model.

Figure 4.11 presents the profiles of mean stream–wise velocities at three x–locations. As can be observed, a strong velocity deficit in the $\bar{u}$–profile occurs in the recirculation region at $x/D = 1.06$ with a U–shape close to the cylinder which evolves toward a V–shape further downstream. The agreement between the current LES and experimental velocity profiles is very satisfactory compared with previous LES studies [51, 53, 54]. However, the pronounced peak of $\bar{u}$ at the edge of the wake region is slightly over–predicted by the DSM.

Figure 4.12 demonstrates the shear–stress profiles at the near wake region. The RAST model results are in a better agreement with the experiment. To summarize for all profiles presented herein, the agreement between the present computations and experimental data is very satisfactory and comparable with the previous LES studies. The small lack of symmetry in the time-averaged values are related to the fact that averaging was not performed in the span-wise direction. These asymmetries are small and are localized to areas where the first or second-order quantity has very small magnitude.

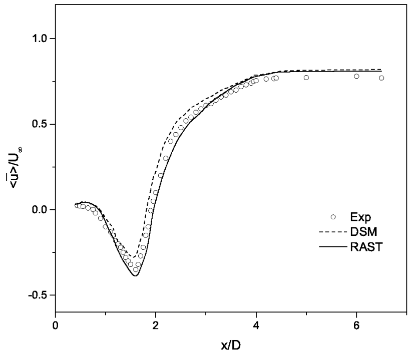

Figure 4.10. Mean stream–wise velocity on centerline.

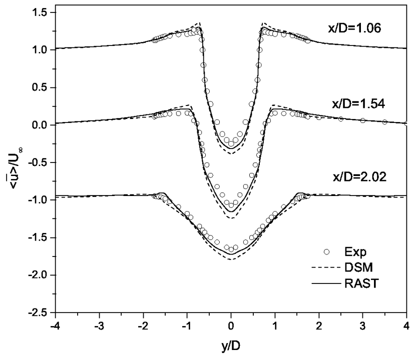

Figure 4.11. Mean stream–wise velocity at different locations near wake of the cylinder (curve shifts are due to an under-prediction of the turbulent viscosity).

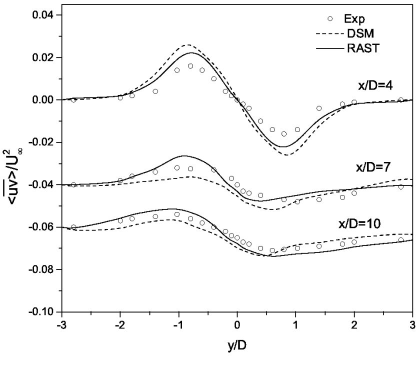

Figure 4.12. Shear stress at different locations at the wake of the cylinder.

4.4 Jet impingement on a curved surface

The performance of a zero-equation model in predicting the jet impingement on a concave surface is discussed in this section. A full description of the computational procedure and the boundary conditions for this case is addressed in Publication III. The computational domain for an unconfined impinging jet on a semi-circular concave surface is utilized according to the experimental setting of Choi et al. [55]. The jet is injected from a rectangular slot with a width of $B = 5$ mm impinging on a curved surface with a diameter of $D = 150$ mm.

A no–slip condition is imposed on the wall and a constant heat flux of 5000 $\mathrm{W/m^2}$ is applied on the impingement surface. The jet inlet temperature (T_i) is set to 300K and the inlet condition at the jet exit is constructed from a separate calculation of a turbulent channel flow with the same width as the inlet slot. A pressure boundary condition is used at the outlets in order to recreate the experimental settings. In the span-wise direction a periodic boundary condition is applied. In order to provide a fully developed turbulent flow condition at the nozzle exit, the nozzle duct is extended for $20B$.

The predicted mean axial velocity at different h/B ratios is represented in Figure 4.13 at $Re = 2960$. The velocity values are normalized with the jet exit velocity U_e and r/B is the normalized distance from the jet exit towards the impingement surface along the jet centerline. As can be seen, DSM over-estimates the velocity close to the impinging zone. As the jet-to-surface distance is increased, a better agreement between the predicted results and the experiment has been achieved. This behaviour can also be seen at $Re = 4740$ for all three applied models (Publication III). By examining the velocity profile in a free jet region especially at lower h/B values, it can be seen that DSM under-estimates the velocity profiles; this may be due to an over-estimation of the turbulent viscosity values at that location.

Figure 4.14 shows the mean velocity profiles at different circumferential locations for $h/B = 6$. The results are compared with the available experimental data at $Re = 2960$ along the radial direction (s). As the flow expands radially along the concave surface, the predicted results become closer to the measured values. It can be seen that DSM over-estimates the values close to the wall jet region especially at $s/B = 4$ and $s/B = 6$, while away from the concave surface these values are under-estimated. Again, here, it should be noted that as the jet-to-surface distance spacing is increased, the predictions of velocity in the wall jet region are in a better agreement with the experiment.

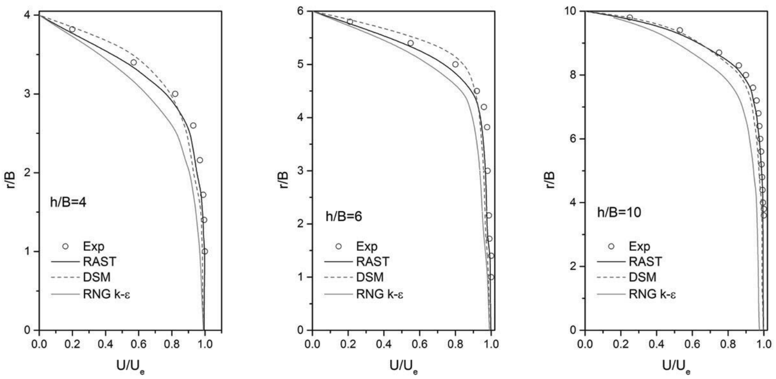

Figure 4.13. Mean axial velocity profiles along the jet centerline at Re =2960.

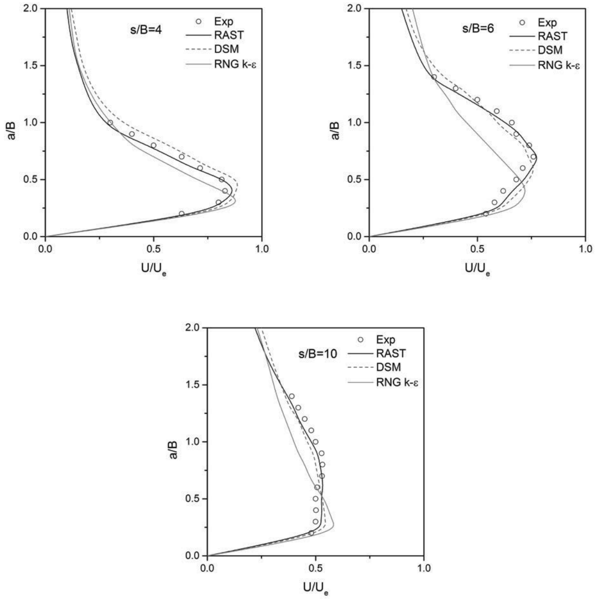

Figure 4.14. Mean velocity profiles along the radial direction at different circumferential location for h/B= 6 at Re = 2960.

5. Conclusions

Two new subgrid scale models for large eddy simulation have been developed in this thesis. These models benefit from a variable eddy viscosity coefficient that depends non–linearly on both the rotational and irrotational strains. This "dynamic" eddy viscosity coefficient C_μ offers some improvements over the traditional SGS models in LES. The main features of these two models are that unlike conventional SGS models e.g. the dynamic Smagorinsky model, they only require a single filtering operation in order to extract the sub-grid turbulent structures and the coefficient C_μ embedded with these models provides a natural damping in the vicinity of the wall.

The underlying mechanism in C_μ effectively reflects the influence of resolved scales on the small ones. This scheme allows the model to adapt itself to the rapid change in the flow topology especially in regions with large strain and rotation rate. The zero-equation model accounts for the sub–grid scale kinetic energy, (k_{sgs}) in which the included coefficient C_μ allows k_{sgs} for an inherent ability to adapt to the local level of turbulent activity to some extent. However, in the one-equation model which is the improved version of a zero-equation model, k_{sgs} is obtained by solving an additional transport equation for k_{sgs}. This turbulent kinetic energy transport equation accounts for the history and non–local effects, having the potential to benefit complex flows with non–equilibrium turbulence as supported by presented numerical test cases.

The performance of both model is somewhat similar. However, the predictions for turbulent channel and diffuser flows by present models demonstrate that the ability of one-equation model to reproduce accurate information on the fluid flow is slightly better than those of a zero-equation model. These models offer a simple and robust expression in the SGS modeling which is easy to implement and cost effective. Computations show that the models are competitive with the dynamic Smagorinsky model and can save up to 20-30% calculation time in similar conditions.

For the future work, due to their ability of being easily implemented, these models can be used in collaboration with the Detached Eddy Simulation (DES) and hybrid RANS–LES modeling. Therefore, according to the nature of the DES method in utilizing both the RANS (close to the wall) and LES, the proposed SGS models can provide a good compromise between robustness and accuracy in various industrial fluid engineering problems where a precise as well as a robust solution is desirable.

Bibliography

[1] H. Tennekes and J.J. Lumley. A First Course in Turbulence. MIT Press, 1972.

[2] O. Reynolds. On the dynamical theory of turbulent incompressible viscous fluids and the determination of the criterion. Philosophical Transactions of the Royal Society of London A, 186:123–161, 1894.

[3] L.F. Richardson. Weather Prediction by Numerical Process. Cambridge University Press, 1922.

[4] A.N. Kolmogorov. The local structure of turbulence in incompressible viscous fluid for very large Reynolds number. Dokl. Acad. Nauk. SSSR, 30: 9–13, 1941.

[5] J. Boussinesq. Theorie d l'ecoulelement tourbillant, volume 1. Mem. Pres., 1877.

[6] L. Prandtl. Uber die ausgebildete turbulenz. Z. Angewandte Mathematik und Mechanik, 5: 136-139, 1925.

[7] B.S. Baldwin and H. Lomax. Thin-layer approximation and algebraic mo del for separated turbulent flows. AIAA Journal, 16: 78-257, 1978.

[8] T. Cebeci. Turbulence models and their application: efficient numerical methods with computer programs. Springer-Verlag, 2004.

[9] P.R. Spalart and S.R. Allmaras. A one-equation turbulence model for aerodynamic flows. AIAA Paper No. 92-0439, 1992.

[10] M.M. Rahman, T. Siikonen and R.K. Agarwal, Improved Low Re-Number One-Equation Turbulence Model, AIAA Journal, Vol. 49 (4): 735-747, 2011.

[11] A. N. Kolmogorov. Equations of turbulent motion of an incompressible fluid. Izvestia Academy of Science, USSR, Physics, 6: 56–58, 1942.

[12] D. C. Wilcox. Turbulence Modeling for CFD. La Canada: DCW Industries, 3rd edition, 2006.

[13] W.P. Jones and B.E. Launder. The prediction of laminarization with a two-equation model of turbulence. International Journal of Heat and Mass Transfer, 15: 301–314, 1972.

[14] B.E. Launder and B.I. Sharma, Application of the Energy Dissipation Model of Turbulence to the Calculation of Flow Near a Spinning Disc, Letters in Heat and Mass Transfer, 1 (2): 131-138, 1974.

[15] V. Yakhot, S.A. Orszag, S. Thangam, T.B. Gatski and C.G. Speziale, Development of turbulence models for shear flows by a double expansion technique, Physics of Fluids A, 4 (7): 1510-1520, 1992.

[16] M. Lesieur, O. Metais and P. Comte. Large-Eddy Simulations of Turbulence. Cambridge University Press, ISBN:9780521781244, 2005.

[17] J. Smagorinsky. General circulation experiments with the primitive equations. i. the basic experiment. Monthly Weather Review, 91 (3): 99-164, 1963.

[18] J.W. Deardorff. A numerical study of three-dimensional turbulent channel flow at large Reynolds numbers. Journal of Fluid Mechanics, 41: 453-480, 1970.

[19] U. Schumann. Subgrid scale model for finite difference simulations of turbulent flows in plane channels and annuli. Journal of Computational Physics, 18: 376-404, 1975.

[20] J. Bardina, J.H. Ferziger, and W.C. Reynolds. Improved subgrid scale models for large eddy simulation.13th fluid and plasma dynamics conference. DOI: 10.2514/6.1980-1357, 1980.

[21] S. Pope. Turbulent Flows. Cambridge University Press, 2000.

[22] E.R. Van Driest. On the turbulent flow near a wall. Journal of the Aeronautical Sciences, 23 (11): 107-1011, 1956.

[23] J.A. Domaradzki and W. Liu. Approximation of subgrid-scale energy transfer based on the dynamics of resolved scales of turbulence. Physics of Fluids, 7: 2025-2035, 1995.

[24] C. Meneveau and J. Katz. Scale-invariance and turbulence models for large-eddy simulation. Annual Review of Fluid Mechanics, 32: 1-32, 2000.

[25] M. Germano, U. Piomelli, P. Moin, and W.H. Cabot. A dynamic subgrid-scale eddy viscosity model. Physics of Fluids, 3: 1760-1765, 1991.

[26] D.K. Lilly, A proposed modification of the Germano subgrid-scale closure model, Physics of Fluids, 4(3): 633-635, 1992.

[27] F. Nicoud and F. Ducros. Subgrid-scale stress modeling based on the square of the velocity gradient tensor, Flow, Turbulence and Combustion, 62: 183-200, 1999.

[28] A.W. Vreman, An eddy-viscosity subgrid-scale model for turbulent shear flow: algebraic theory and applications, Physics of Fluids, 16 (10): 3670–3681, 2004.

[29] A. Leonard. Energy cascade in large-eddy simulations of turbulent fluid flows. Advances in Geophysics, 18: 237-248, 1974.

[30] R.A. Clark, J.H. Ferziger, and W.C. Reynolds. Evaluation of subgrid scale models using an accurately simulated turbulent flow. Journal of Fluid Mechanics, 91: 1-16, 1979.

[31] M.M. Rahman and T. Siikonen. An explicit algebraic Reynolds stress model in turbulence. International Journal of Numerical Methods in Fluids, 52: 1135–1157, 2006.

[32] W. Kim and S. Menon. Application of the localized dynamic subgrid scale model to turbulent wall–bounded flows. AIAA Paper No. 97-0210, 1997.

[33] A. Yoshizawa. Statistical theory for compressible turbulent shear flows, with the application to subgrid modeling. Physics of Fluids, 29 (7): 2152–2164, 1986.

[34] J.L. Lumley. Computational modeling of turbulent flows. Advances in Applied Mechanics, 18: 124–176, 1978.

[35] M.M. Rahman and T. Siikonen. An eddy viscosity model with near–wall modifications. International Journal of Numerical Methods in Fluids, 49: 975–997, 2005.

[36] M.M. Rahman and T. Siikonen. A low–Reynolds number explicit algebraic stress model. ASME Journal of Fluids Engineering, 128: 1364–1376, 2006.

[37] B. Vreman, B. Geurts and H. Kuerten. Realizability conditions for the turbulent stress tensor in large-eddy simulation. Journal of Fluid Mechanics, 278: 351-362, 1994.

[38] R.D. Moser, J. Kim and N.M. Mansour. Direct numerical simulation of turbulent channel flow. Physics of Fluids, 11: 943–945, 1999.

[39] P.P. Sullivan, J.C. McWilliams and C.H. Moeng. A subgrid scale model for large eddy simulation of planetary boundary–layer flows. Boundary–layer Meteorology, 71: 247–276, 1994.

[40] J.B. Cazalbou and P. Bradshaw. Turbulent transport in wall bounded flows. Evaluation of model coefficients using direct numerical simulation. Physics of Fluids, 5: 3233–3239, 1993.

[41] K. Horiuti. Large eddy simulation of turbulent channel flow by one–equation modeling. Journal of the Physical Society of Japan, 54: 2855–2865, 1985.

[42] J. Taghinia, M.M. Rahman and T. Siikonen. Numerical simulation of airflow and temperature fields around an occupant in indoor environment. Energy & Buildings, 104: 199–207, 2015.

[43] P.K. Yeung and Y. Zhou. Universality of the Kolmogorov constant in numerical simulation of turbulence. Physical Review E, 56: 1746–1752, 1997.

[44] C.M. Winkler and L.R. Sarma. Evaluation of subgrid scale kinetic energy models in large eddy simulations of turbulent channel flow. International Journal of Numerical Methods for Heat and Fluid Flow, 2: 226–239, 2006.

[45] D. You and P. Moin. A dynamic global-coefficient subgrid-scale model for large-eddy simulation of turbulent scalar transport in complex geometries. Physics of Fluids, 21, 045109, 2009.

[46] A. Rasam, G. Brethouwer and A. V. Johansson. An explicit algebraic model for the subgrid-scale passive scalar flux, Journal Fluid Mechanics, 721: 541–577, 2013.

[47] S. Singh and D. You. A dynamic global-coefficient mixed subgrid-scale model for large-eddy simulation of turbulent flows. International Journal of Heat and Fluid Flow, 42: 94–104, 2013.

[48] C. Hartel and Leonhard Kleiser. Analysis and modelling of subgrid-scale motions in near-wall turbulence. Journal of Fluid Mechanics, 356: 327- 352, 1998.

[49] P.V. Nielsen, A. Restivo and J.H. Whitelaw. The velocity characteristics of ventilated room. ASME Journal of Fluids Engineering, 100: 291–298, 1978.

[50] U. Piomelli. Large-eddy simulation: achievements and challenges. Progress in Aerospace Sciences, 35: 335-362, 1999.

[51] J. Franke and W. Frank. Large Eddy simulation of the flow past a circular cylinder at Re_D=3900. Journal of Wind Engineering and Industrial Aerodynamics, 90: 1191–1206, 2002.

[52] L.M. Lourenco and C. Shih. Characteristics of the plane turbulent near wake of a circular cylinder. A particle image velocimetry study. 1993, (data taken from Beaudan and Moin(1994))

[53] M. Breuer. Large Eddy simulation of the sub-critical flow past a circular cylinder: numerical and modeling aspects. International Journal of Numerical Methods in Fluids, 28: 1281-1302, 1998.

[54] P. Parnaudea, J. Carlier D. Heitz and E. Lamballais. Experimental and numerical studies of the flow over a circular cylinder at Reynolds number 3900. Physics of Fluids, 20: 085101(1–13), 2008.

[55] M. Choi, H.S. Yoo, G. Yang, J.S. Lee and D.K. Sohn, Measurement of impinging jet flow and heat transfer on a semi-circular concave surface. International Journal of Heat and Mass Transfer, 43: 1811–1822, 2000.

Aalto-DD 195/2015

"I am an old man now, and when I die and go to heaven there are two matters on which I hope for enlightenment. One is quantum electrodynamics, and the other is the turbulent motion of fluids. And about the former I am rather optimistic."

-Horace Lamb (1849-1934)

ISBN 978-952-60-6534-2 (printed)
ISBN 978-952-60-6533-5 (pdf)
ISSN-L 1799-4934
ISSN 1799-4934 (printed)
ISSN 1799-4942 (pdf)

Aalto University
School of Engineering
Department of Applied Mechanics
www.aalto.fi

BUSINESS +
ECONOMY

ART +
DESIGN +
ARCHITECTURE

SCIENCE +
TECHNOLOGY

CROSSOVER

DOCTORAL
DISSERTATIONS